Open access • Journal Article • DOI:10.1039/C1JM11832C

Nanocomposites of a nematic liquid crystal doped with magic-sized CdSe quantum dots — Source link

Javad Mirzaei, Martin Urbanski, Kui Yu, Heinz-S. Kitzerow ...+1 more authors

Institutions: University of Manitoba, University of Paderborn, National Research Council

Published on: 16 Aug 2011 - Journal of Materials Chemistry (The Royal Society of Chemistry)

Topics: Liquid crystal, Homeotropic alignment and Quantum dot

Nanocomposites of a nematic liquid crystal doped with magic-sized CdSe quantum dots

Mirzaei, Javad; Urbanski, Martin; Yu, Kui; Kitzerow, Heinz-S.; Hegmann, Torsten

Publisher's version / Version de l'éditeur:
https://doi.org/10.1039/C1JM11832C
Journal of Materials Chemistry, 21, 34, pp. 12710-12716, 2011-07-26

Journal of Materials Chemistry

Cite this: J. Mater. Chem., 2011, 21, 12710

www.rsc.org/materials

PAPER

Nanocomposites of a nematic liquid crystal doped with magic-sized CdSe quantum dots†

Javad Mirzaei,[a] Martin Urbanski,[b] Kui Yu,[c] Heinz-S. Kitzerow[b] and Torsten Hegmann*[a]

Received 26th April 2011, Accepted 22nd June 2011
DOI: 10.1039/c1jm11832c

We here report on the optical, alignment and electro-optic properties of a nematic liquid crystal affected by the presence of semiconductor CdSe magic-sized nanocrystals (MSNCs). Three single-sized CdSe samples were tested, exhibiting bright bandgap photoluminescence (PL) with $\lambda_{max} \approx 463$ nm and ~10 nm full width at half-maximum (fwhm). The three quantum dot (QD) samples were passivated with a monolayer of myristic acid. Two of them (**QD1** and **QD2**) only vary in the amount of defects as indicated by different bandgap and deep trap PL. The third MSNC sample (**QD3**) is compositionally different, doped with Zn. These MSNCs with almost identical sizes were doped at different concentrations (1–5 wt%) into the nematic phase of 5-*n*-heptyl-2-(4-*n*-octyloxyphenyl)-pyrimidine (**LC1**). Only **QD3** showed the formation of birefringent stripes surrounded by areas of homeotropic alignment between plain glass slides at all concentrations as observed for many other nanoparticle-doped nematic liquid crystals reported earlier by our group. In polyimide-coated glass slides favouring planar orientation of the nematic director, planar alignment was observed. Surprisingly, only the Zn-doped magic-sized **QD3** quantum dots (CdSe@Zn) significantly lower the dielectric anisotropy as well as the splay elastic constant of the nematic host, despite identical size and surface functionality, which highlights the tremendous effect of the nanocrystal core composition on the electro-optic properties of the nematic host. In addition, fluorescence confocal (polarizing) microscopy studies show the director field within and around the birefringent stripes and confirm locally elevated concentrations or aggregates of the MCNC that are otherwise randomly distributed in the nematic host.

Introduction

Doping, *i.e.* the intentional incorporation of small quantities of an additive into a nematic liquid crystal (N-LC), is one of the most prominent processes to tune both the optical and electro-optical properties of anisotropic nematic fluids.

The response of a nematic liquid crystal such as **LC1** (Scheme 1) to an applied electric field is an important property in the application of N-LCs in many optical devices such as liquid crystal displays (LCDs). The ability of the director (parallel to the long molecular axis for a rod-like N-LC) to align along an external field results from permanent or induced electric dipoles within the molecules.

Pure LCs or custom LC mixtures for LCD applications are generally desirable with low threshold voltage (V_{th}) and maximal dielectric anisotropy $\Delta\varepsilon$ ($\Delta\varepsilon = \varepsilon_{\parallel} - \varepsilon_{\perp}$, where $\varepsilon_{\parallel}$ is the electrical permittivity along the long molecular axis and $\varepsilon_{\perp}$ the electrical permittivity perpendicular to $\varepsilon_{\parallel}$), either positive or negative, along with low viscosity and short switching times (rise and fall times). For an N-LC such as **LC1** in a planar, rubbed polyimide-coated cell, the splay elastic constant (K_{11}) is also of significance.

Splay is the deformation that arises when an electric field is applied to such cell.[1] Above V_{th}, the director gradually reorients from a planar orientation near the alignment layers to a vertical (or homeotropic) orientation in the bulk of the LC film in the so-called Freedericksz transition.

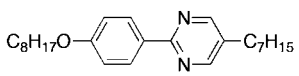

LC1; Phase sequence: Cr - 52°C (SmA - 45°C) - N - 70°C - Iso

Scheme 1 Chemical structure and phase transition temperatures of LC1 (Cr = crystalline solid, SmA = smectic-A phase, N = nematic phase, Iso = isotropic liquid).

[a]*Department of Chemistry, University of Manitoba, Winnipeg, MB, R3T 2N2, Canada. E-mail: hegmannt@cc.umanitoba.ca; Fax: +1 204 474 7608; Tel: +1 204 474 7535*
[b]*Department of Chemistry, University of Paderborn, Paderborn, Germany. E-mail: heinz.kitzerow@upb.de; Fax: +49 (0) 5251 604 208; Tel: +49 (0) 5251 602 156*
[c]*Steacie Institute for Molecular Sciences, National Research Council of Canada, Ottawa, ON, K1A 0R6, Canada. E-mail: Kui.Yu@nrc-cnrc.gc.ca*

† Electronic supplementary information (ESI) available: UV-vis spectra, XPS data of the quantum dots, additional FCPM images, transmission *vs.* applied voltage plots (also at different frequencies of the applied electric field), as well as plots of electric permittivities and specific resistivities *vs.* reduced temperature. See DOI: 10.1039/c1jm11832c

K_{11}, as shown in eqn (1) below, is directly proportional to V_{th}^2 and $\Delta\varepsilon$.[1]

$$K_{11} = (V_{th}/\pi)^2 \varepsilon_0 |\Delta\varepsilon|, \quad (1)$$

where ε_0 is the permittivity of free space.

Doping LCs with colloidal particles such as aerosols,[2–5] or more recently with nanoscale materials such as carbon nanotubes[6–11] or quasi-spherical nanoparticles (NPs) is an active interdisciplinary research topic attracting interest from both academia and industry since such suspensions exhibit striking properties not observed for pure LCs or LC mixtures. For example, changing the optical behaviour by imposing discrete alignment modes different from the corresponding non-doped LC, generating rheological changes due to topological defects, improving response times, and lowering of V_{th} values have all been reported for N-LCs doped with metal-based, ferroelectric, dielectric or semiconductor NPs, among others.[12–25] However, irreversible aggregation or phase separation or segregation of NPs in the LC host as well as defect formation induced by the presence of NPs were often either neglected, difficult to ascertain, or did simply not result in a visualizable or measurable event or effect. Earlier work from our group on the other hand has frequently described multiple alignment modes and defect textures due to NP segregation along with lower V_{th} (as a result thereof), altered elastic constants, and dielectric properties in N-LCs doped with alkylthiol-capped gold NPs as well as CdSe and CdTe quantum dots (QDs).[12,25–27]

QDs were particularly attractive for addressing the problem of larger size distributions known to arise from the synthesis of gold NPs and particularly for investigating trends in the effects of NP size and surface functionality (non-polar aliphatic *vs.* polar) in N-LCs. An important piece of the puzzle still missing to gain a more complete understanding of NP–LC interactions is the use of truly monodisperse NPs, which, in a series, would ideally differ in one or more parameter such as core composition or coating.

Building on our earlier data on NP doped N-LCs including the formation of electrohydrodynamic instabilities (*i.e.* convection rolls or Kapustin-Williams domains),[26,28,29] we here present new, detailed data from optical (textures and defects), electro-optic as well as alignment studies using magic-sized QDs with very low polydispersity index as dopants in the N-LC host **LC1** (frequently used in earlier studies). To demonstrate effects of small changes in QD surface disorder or the QD surface composition on the optical, electro-optic and alignment properties of **LC1**, we selected three CdSe QDs with **QD1**[30] and **QD2**[31] only differing in the degree of surface defect states (indicated by differences in deep trap PL emission) due to an altered preparation procedure, and **QD3** (ref. 32) differing from the other two by Zn doping, CdSe@Zn. All three QDs are quasi identical in core size and are consistently capped, in principle, with the same fatty acid (*i.e.* myristic acid).

The strong, narrow bandgap PL emission of these QDs (Fig. 1) was also used in fluorescence confocal polarizing microscopy (FCPM) experiments to determine the distribution of the QDs in the N-LC as well as their aggregation and segregation behaviour. Several of these imaging studies were performed in conjunction with a dichroic dye (*vide infra*) to clarify LC alignment as well as director fields within or around defects using plain glass or rubbed polyimide ITO-coated glass cells.

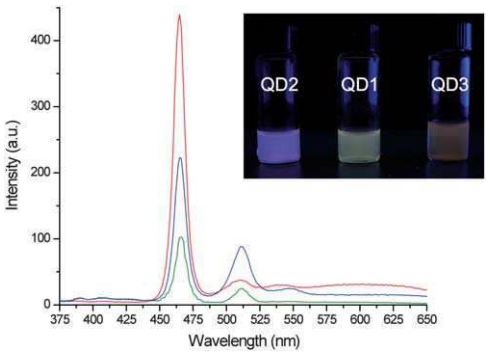

Fig. 1 PL emission spectra ($\lambda_{exc} = 400$ nm) of magic-sized quantum dots **QD1** (blue spectrum), **QD2** (green spectrum), and **QD3** (red spectrum) in toluene. The spectra were normalized with the same optical density at the excitation wavelength. Note that compared to **QD2**, **QD1** exhibits relatively enhanced deep trap emission, while **QD3** much decreased deep trap emission at ~512 nm (with respect to the bandgap emission at ~463 nm) as a result of the Zn doping (Inset: **QD1**-**QD3** in toluene).

Experimental section

Materials and methods

LC1 was used as received from Synthon Chemicals GmbH. The three QDs (**QD1–QD3**) were prepared using a non-injection, one-pot synthesis as reported earlier,[30–32] using $Cd(OAc)_2 \cdot 2H_2O$, Se, and Zn (for **QD3** only)[32] in 1-octadecene in the presence of myristic acid ($CH_3(CH_2)_{12}CO_2H$) and trioctylphosphine (TOP) in a small quantity (to activate Se) as surface ligands (see Table 1).

Photoluminescence spectra were collected using a Varian Cary Eclipse (λ_{exc} = 400 nm). UV-vis spectra were collected using a Varian Cary 5000 UV-vis-NIR spectrophotometer (see the ESI† for absorption spectra of the three QDs).

The mixtures of the CdSe quantum dots in **LC1** were prepared by weighing accurate amounts of the solid LC using a microbalance and dissolving it in a known amount of toluene for **QD1** and **QD2** or hexane for **QD3**. The toluene solutions of the **QD1** and **QD2** QDs and the hexane solution of CdSe@Zn QDs (**QD3**) were combined in a V-vial® with the LC solution to produce the exact concentration of the QDs in **LC1** (1, 2.5 and 5 wt% mixtures).

The solvent was then allowed to evaporate under a steady stream of dry N_2 at ~70 °C for about 24–48 h followed by sonication. The importance of direct, pulsed sonication using a sonotrode (output power: 750 W, $f = 20$ kHz, 5 s ON then 5 s OFF at an output power amplitude of 21%) is demonstrated in the ESI†.

Polarized optical microscopy (POM) images were taken using an Olympus BX51-P polarized optical microscope in conjunction with a Linkam LS350 heating/cooling stage. Electro-optic (EO) analysis was performed using an LCAS 1 automated liquid crystal analyzer (LC Vision). EO data were obtained using the single-cell method built into the LCAS 1 software as originally

Table 1 Size-distribution of magic-sized QDs (**QD1–QD3**)[a]

QD*x*	Size ± SD/diameter nm^{-1}	Capping agent
QD1 (CdSe)[29]	2.0 ± 0.1[b] (quasi-spherical)	$CH_3(CH_2)_{12}COOH$
QD2 (CdSe)[30]	2.0 ± 0.1[b] (quasi-spherical)	$CH_3(CH_2)_{12}COOH$[c]
QD3 (CdSe@Zn)[31]	2.0 ± 0.1[b] (quasi-spherical)	$CH_3(CH_2)_{12}COOH$[c]

[a] Calculated from the 1st excitonic absorption peak position. [b] On TEM grids, some aggregation after solvent evaporation leads to larger QD assemblies, which can be broken up by re-dispersing them in toluene or hexane. Size distributions as small as 0.1 nm (as calculated from spectroscopic data) are difficult to estimate by TEM image analysis. [c] The surface of these QDs is simultaneously capped with myristic acid and a small percentage of TOP (trioctylphosphine) used to 'activate' Se. For more details, see ref. 30–32. For XPS data, see ESI†.

described by Wu *et al.*[33] The LC test cells used were planar 4.0 μm cells with antiparallel polyimide alignment layers and 1° to 3° pre-tilt (LC Vision). For all POM imaging and EO measurements, the LC mixtures were heated above the isotropic/nematic phase transition temperature ($T_{Iso–N}$) and cooled at a rate of 1 °C min^{-1} until the desired temperature below $T_{Iso–N}$ was reached. The average of all values and standard deviations of each electro-optic parameter were calculated from at least five or up to ten measurements at any given temperature for each mixture (also using different cells). FCPM images were obtained using a Nikon LV 100D-U upright microscope coupled with a Nikon Eclipse C1 Plus scanner/controller using two excitation lasers; $\lambda_{excI} = 408$ nm to excite the QDs and $\lambda_{excII} = 488$ nm to excite the dichroic dye *N*,*N*′-bis(2,5-di-*tert*-butylphenyl)-3,4,9,10-perylenedicarboximide (obtained from Aldrich) used at 0.001 wt%. The dye shows a bright fluorescence at $\lambda = 540$ nm that was easily separated from the PL emission of the QDs using a beam splitter cube or interference beam splitter as well as by-pass filters. Moreover, for some experiments, the microscope was equipped with a polarizer, a quarter wave plate, and an analyzer for polarization control.

Results and discussion

Polarized light optical microscopy (POM)

POM investigations, as in all earlier studies on NP-doped N-LCs, are always the starting point for further optical and electro-optic measurements. POM provides first clues on the aggregation and segregation behaviour of the NPs dispersed in the N-LC host. The formation of characteristic birefringent stripe defects as well as the temperature-dependent induction of homeotropic alignment for several N-LC hosts despite the presence of surfaces known to promote planar alignment were frequently observed in our lab for NP-doped mixtures showing the most drastic changes of the EO properties. Most likely, altered EO properties were observed as a consequence of these aggregation and segregation phenomena.

Hence, all mixtures were first studied by POM between plain, untreated microscopy glass slides and then in rubbed polyimide-coated, ITO-glass cells promoting planar alignment. Fig. 2–4 show optical photomicrographs of textures observed between plain glass slides (a–c) and the alignment as well as defects in planar EO cells (d–f) of **LC1** doped with **QD1–QD3** at 1, 2.5, and 5 wt%. A close inspection of these images reveals the first major differences in the behaviour of the three QDs in **LC1**.

Both **QD1** and **QD2** in **LC1** mainly show *schlieren* textures between plain glass slides (with the exception of the 2.5 wt% **QD1** in **LC1** mixture showing the typical birefringent stripe texture). **QD3**, however, only shows homeotropic alignment with an increasing area density of birefringent stripe defects usually observed by our group for NP-doped N-LCs.

This observation provides the first important hint that **QD1** and **QD2** are significantly better miscible with the N-LC host, and that **QD3** segregates to the LC–glass interfaces (top and/or bottom) inducing homeotropic alignment of the director on plain glass. The same trend is also observed in rubbed polyimide-coated ITO-glass cells (thickness: 4 μm). Mixtures of **LC1** doped with **QD1** and **QD2** show relatively defect-free planar alignment with some point-like defects (not exclusively caused by spacers), which in some cases follow the rubbing direction of the cell (see both images of 5 wt% **QD1** or **QD2** in **LC1** in Fig. 2f and 3f). These circular, point-like defects are most likely caused by minor aggregation of the QDs in the N-LC film (very pronounced for 2.5 wt% of **QD2** in **LC1** in Fig. 3e). Results of FCPM imaging discussed in the ESI† shine more light onto the origin of these defects. **QD3**, however, notably distorts the homogeneous planar alignment of **LC1** in planar cells (Fig. 4d–f). Here, just 1 wt% of **QD3** in **LC1** produces quasi chain-like networks of point defects (similar to the highest concentrations of **QD1** and **QD2** in **LC1**). Increasing the amount of **QD3** in **LC1** initially produces defect domains with reduced birefringence (Fig. 4e, at 2.5 wt%) and at 5 wt% a network of defects with homeotropic alignment (Fig. 4f). These homeotropic areas are probably caused by a combination of some QD aggregation and most certainly by QD segregation to the alignment layer–LC interface.

However, major aggregation of the QDs in all mixtures with **LC1** is not observed as can be seen in the images with parallel, un-crossed polarizers. With respect to their optical behaviour in thin films, both **QD1** and **QD2** in **LC1** behave similar to hydrophilic CdTe QDs capped with thioglycolic acid ranging in size from 3.2 to 4.0 nm,[25] and **QD3** similar to alkylthiol-capped gold NPs of similar size[12] and hydrophobic CdSe QDs capped

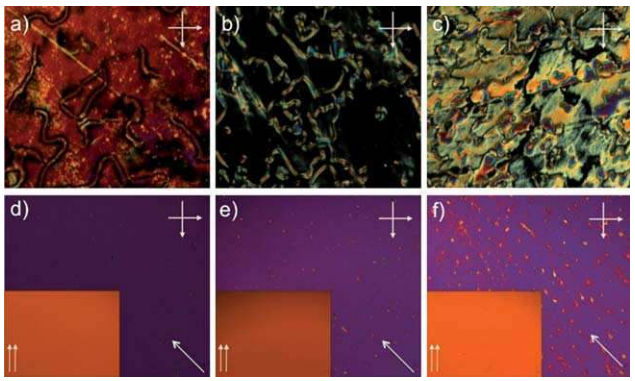

Fig. 2 POM photomicrographs (crossed polarizers) of **LC1** doped with **QD1** at $T_{Iso–N} - T = 9$ °C (top, (a–c): plain glass; bottom, (d–f): 4.0 μm anti-parallel planar cell): (a and d) 1 wt%, (b and e) 2.5 wt%, (c and f) 5 wt%. White arrows in the bottom right corner in (d–f) show the rubbing direction of the cell, and the inset in (d–f) shows the same area with parallel polarizers.

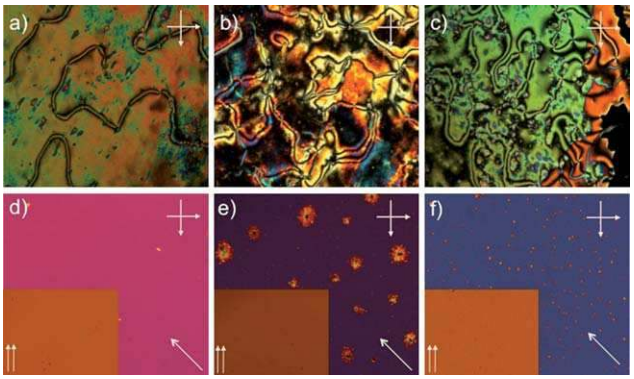

Fig. 3 POM photomicrographs (crossed polarizers) of **LC1** doped with **QD2** at $T_{Iso–N} - T = 9$ °C (for details, see caption to Fig. 2).

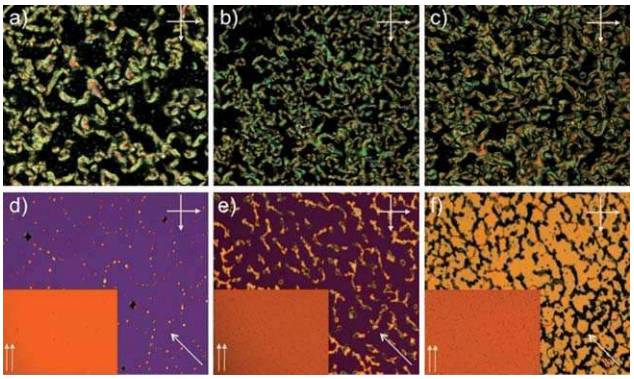

Fig. 4 POM photomicrographs (crossed polarizers) of **LC1** doped with **QD3** at $T_{Iso–N} - T = 9$ °C (for details, see caption to Fig. 2).

with hexadecylamine ranging in size from 2.5 to 5.2 nm reported earlier (the latter only at lower concentrations, *i.e.* 1 wt%).[25]

The difference in alignment, texture and defect behaviour is all the more significant considering that Zn doping for **QD3** is the only difference to **QD1** and **QD2** with all other parameters such as size and monolayer capping kept largely constant.

Electro-optic (EO) characterization

To see if this difference in defect formation between **QD1/QD2** and **QD3** in **LC1** affects the response of this N-LC host to an applied electric field, we next performed detailed electro-optic tests (*i.e.* measuring the capacity *vs.* applied voltage) using the single-cell method described in the Experimental section.

Rather surprisingly, considering most of our earlier work on Au NPs and QDs in **LC1**,[25–27] data collected in Fig. 5 show that none of the QDs exerts any significant effect on V_{th} of **LC1** over the investigated concentration range up to 5 wt%. Only at 5 wt%, and at temperatures well below the Iso–N phase transition, the slope of V_{th} *vs.* $T/T_{Iso–N}$ begins to show a trend to lower values of V_{th}. Transmission *vs.* applied voltage measurements confirm a steady decrease of V_{th} with increasing QD concentration for **QD3** in **LC1**, and show the lowest value of V_{th} for the 2.5 wt% mixture of **QD1** in **LC1** (the mixture with a QD concentration showing a birefringent stripe texture in Fig. 2 (for data plots see ESI†)).[34]

Since nearly all metal NPs and semiconductor QDs capped with hydrophobic hydrocarbon monolayers reduced V_{th} in the past, the question we asked is: do these magic-sized QDs, at that particular size, impart any effect on the electro-optic properties of **LC1**? Plots of the dielectric anisotropy ($\Delta\varepsilon$) *vs.* $T/T_{Iso–N}$ (see Fig. 6) demonstrate that this is indeed the case.

Two unique trends can be seen in these plots. First, increasing the concentration of all three QDs gradually lowers $\Delta\varepsilon$ (little at 1 wt%, but more and more significantly at 2.5 and 5 wt%); with a largely identical slope of $\Delta\varepsilon$ *vs.* $T/T_{Iso–N}$. Second, and particularly striking, the Zn-doped **QD3**, which is compositionally different from **QD1** and **QD2**, induces significantly lower values of $\Delta\varepsilon$ than **QD1** and **QD2**, highlighting that changes in surface composition of these QDs intrinsically or concurrently *via* induced local changes of the alignment in planar EO cells (see alignment defect network in Fig. 4f) can have a considerable effect on the dielectric properties of a given N-LC host.

Considering eqn (1) above, and unaltered values for V_{th} discussed earlier, one would expect that the splay elastic constant, K_{11}, of **LC1** in this cell geometry would also be reduced with an

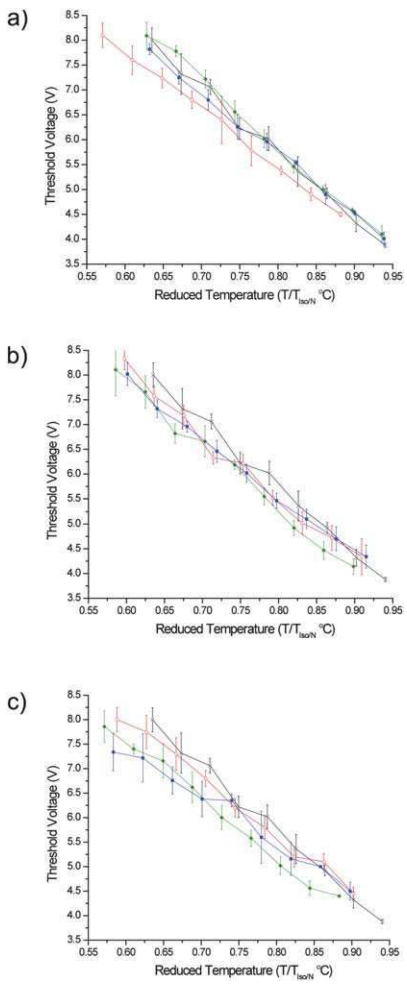

Fig. 5 Plots of the threshold voltage, V_{th} *vs.* the reduced temperature $T/T_{Iso–N}$ (V_{th} was plotted against $T/T_{Iso–N}$ to account for changes in the Iso–N phase transition temperature due to an increasing amount of dispersed QDs) of pure **LC1** (black dataset) as well as **QD1** (blue), **QD2** (green) or **QD3** (red) in **LC1** at: (a) 1 wt%, (b) 2.5 wt%, and (c) 5 wt%.

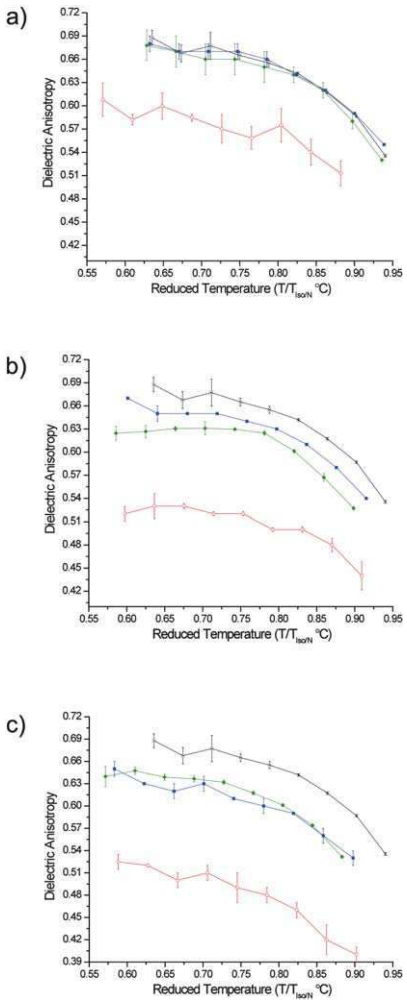

Fig. 6 Plots of the dielectric anisotropy, $\Delta\varepsilon$ *vs.* the reduced temperature $T/T_{\mathrm{Iso-N}}$ of pure **LC1** (black dataset) as well as **QD1** (blue), **QD2** (green) or **QD3** (red) in **LC1** at: (a) 1 wt%, (b) 2.5 wt%, and (c) 5 wt%. $\Delta\varepsilon$ values especially for the 5 wt% sample are affected (*i.e.* slightly higher) because not the entire electric field-addressed area participates in the reorientation.

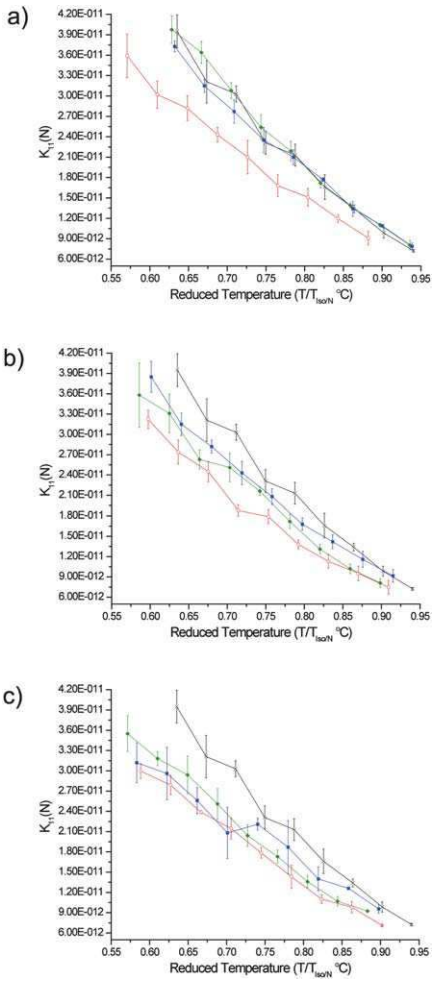

Fig. 7 Plots of the splay elastic constant, K_{11} *vs.* the reduced temperature $T/T_{\mathrm{Iso-N}}$ of pure **LC1** (black dataset) as well as **QD1** (blue), **QD2** (green) or **QD3** (red) in **LC1** at: (a) 1 wt%, (b) 2.5 wt%, and (c) 5 wt%.

increasing concentration of all three QDs. In addition, the most drastic decrease would be expected for **QD3**. Data collected in Fig. 7 confirm this, showing that the two effects, a reduction in $\Delta\varepsilon$ and in K_{11}, cancel each other out. Consequently, the measured V_{th} values are similar to those obtained for pure **LC1**.

Additional electro-optic data such as $\varepsilon_{\parallel}$ and $\varepsilon_{\perp}$ *vs.* $T/T_{\mathrm{Iso-N}}$ as well as transmission *vs.* applied voltage measurements at various frequencies can be found in the ESI†. It is important to note that the decrease in $\Delta\varepsilon$ is caused by a decrease in $\varepsilon_{\parallel}$, with $\varepsilon_{\perp}$ showing values similar to pure **LC1**. Considering all electro-optic measurements, one can conclude that the new magic-sized QDs featuring a much narrower size distribution in comparison to previously examined QDs and Au NPs induce noticeably less significant changes in the electro-optic properties of **LC1**, and most notably no changes in V_{th}. We also noticed, however, that the magic-sized QDs used in the current study appear to be better dispersible (even in the form of aggregates) in **LC1** judging from the texture characteristics between plain glass (with the exception of the Zn-doped **QD3**) and more importantly in planar EO test cells. Only **QD3** significantly reduces both $\Delta\varepsilon$ and K_{11}. **QD3** is the only QD of the three in this series that shows the formation of birefringent stripes between plain glass slides and, at higher concentration, the induction of domains with homeotropic alignment in planar test cells. In this respect, **QD3** behaves similar to previously studied Au NPs[26] featuring almost identical core size and *n*-alkylthiol capping agents with similar alkyl chain length as myristic acid used here ($C_{12}H_{25}SH$ *vs.* $C_{13}H_{27}COOH$).

Fluorescence confocal polarizing microscopy (FCPM)

To obtain more detailed information on the distribution of these magic-sized QDs in films of **LC1** between plain glass slides, we performed FCPM studies. Of specific interest are here mixtures of **QD1** at 2.5 wt% and **QD3** (2.5 wt% are here representative for the entire concentration range) in **LC1**, since only those two QDs showed textures between plain glass slides featuring birefringent stripes and homeotropic alignment in all domains surrounding the stripes.

The emission of the dichroic dye mimicking the director orientation of the nematic LC in these domains[35] and the emission from the QDs are easily separated. The final combined images showing both channels confirm homeotropic alignment of **LC1**, planar alignment of the molecules within the birefringent stripes, as well as the (x–y) distribution of the QDs.

Earlier experiments using larger Au NPs have already shown that these birefringent stripes correspond to twist disclinations located at the substrate interface,[36] and established that larger CdSe QDs (4.0 to 4.3 nm in diameter) segregate to the bottom and top interfaces using (x–z) scans.[37]

Fig. 8 evidently demonstrates the existence of homeotropic alignment in the areas surrounding the birefringent stripes (no dye emission, see Fig. 8b and d). The orientation of the LC director within the birefringent stripes was also confirmed as in our previous work[36] by comparison of linearly polarized scans with a circularly polarized (x–y) scan (see ESI†).

Limited spatial resolution in the z-direction while imaging both channels (*i.e.* dye and QDs), however, prevented us so far from determining the z-distribution of these QDs in contrast to earlier FCPM experiments using larger CdSe QDs,[36] but a more in-depth study is currently underway.

It is important to highlight that all three QDs are generally reasonably well dispersed in **LC1**. Locally elevated PL intensities imaged by confocal microscopy (intense blue signals in Fig. 8b and d) only show that the QDs aggregate in some areas more than in others. The dispersion of the QDs can be demonstrated by adjusting the gain on the PL detector and by using the most suitable aperture of the objective lens. The image in Fig. 9 for 2.5 wt% **QD3** in **LC1** clearly shows that the QDs are dispersed throughout the entire nematic film.

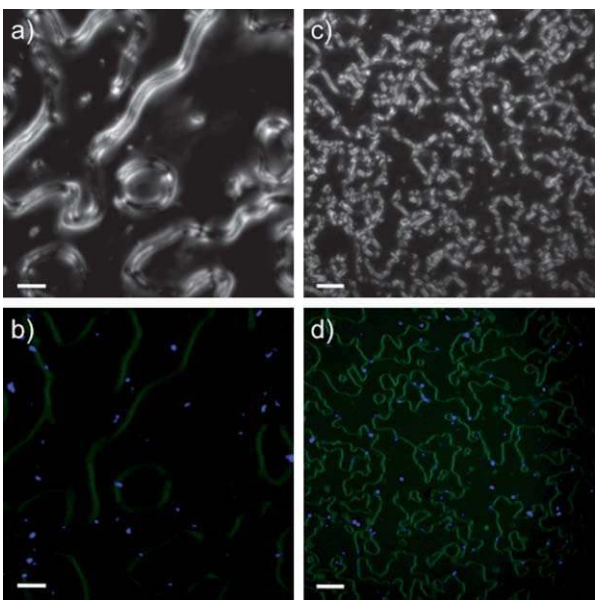

Fig. 8 POM and two-channel FCPM images of 2.5 wt% **QD1** (a and b) and 2.5 wt% **QD3** in **LC1** (c and d). (a and c) Transmission channel (POM); (b and d) (x–y) scan of blue (QD) and green (dye) channel. Scale bars: (a and b) 20 μm; (c and d) 60 μm.

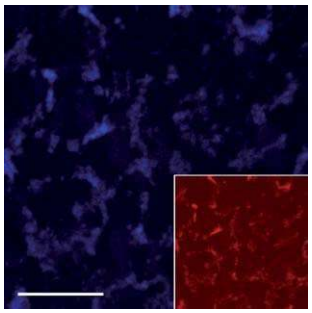

Fig. 9 FCPM image of 2.5 wt% **QD3** in **LC1** (blue channel, *i.e.* **QD3** only). Inset shows a false colour image of the same area with much better contrast. Scale bar: 20 μm.

Conclusions

We have, for the first time, tested if truly monodisperse, so-called magic-sized semiconductor quantum dots can be used as dopants in a nematic LC host to unravel fundamental structure–property relationships governing interactions in LC/NP dispersions.

Three different magic-sized quantum dots were investigated; two differing in surface defect states due to differences in the preparation protocol and very small amounts of TOP on the QD surface in addition to the general monolayer capping of myristic acid, and a third one differing from the other two in the core composition (Zn doping). These quantum dots are smaller in comparison to quantum dots studied previously in the same nematic host,[25] but similar in size to gold nanoparticles with a comparable chain length of the aliphatic capping agent.[26]

Surprisingly, the magic-sized quantum dots investigated here only marginally alter the electro-optic properties, yet some very distinct trends are clearly observable. Only the Zn-doped **QD3** quantum dots, which are core-compositionally different from the other two (**QD1** and **QD2**), affect both the electric permittivity along the long molecular axis of the nematic host (**LC1**), $\varepsilon_{\|}$, and the splay elastic constant K_{11}, but the effects largely cancel each other out with respect to the threshold voltage, V_{th}. Hence, only slightly lower values for V_{th} were observed, both in capacitance and transmission *vs.* applied voltage measurements for **QD3** in **LC1**. **QD3** is also the only of the three quantum dots (and **QD1** at 2.5 wt%—the mixture with the lowest value for V_{th} in transmission *vs.* applied voltage measurements) inducing significant textural changes in **LC1** between plain glass slides as well as in rubbed polyimide-coated ITO/glass cells favouring planar alignment over the entire concentration range (from 1 to 5 wt%). In this respect, only **QD3** behaves similar to alkylthiol-capped gold NPs, which induce homeotropic alignment and the formation of birefringent stripes between plain glass and in planar test cells.[27] In fact, since only **QD3** induces significant alignment changes in some smaller localized domains, as observed by POM, one could conclude that primarily segregation phenomena producing altered alignment scenarios are responsible for significant changes in the electro-optic behaviour of this particular N-LC host. Recent experiments by Goodby *et al.*,[38] however, revealed that both types of NPs, NPs that segregate as in most of our NP-doped mixtures as well as well-miscible, LC-decorated NPs, are capable of inducing sizeable electro-optic effects. Considering the series presented here, differences in the

density of the monolayer capping (or quality of the monolayer) due to variations in surface defect states might well account for the differences in QD miscibility. Future work will now address the role of electroconvection (or perhaps surface polarization effects[39]) as described in previous work from our groups using Au NPs in the same N-LC host.[29,37] Finally, images obtained from FCPM studies (x–y scans) confirm the director field in the birefringent stripes,[36] prove homeotropic alignment in the surrounding domains, show that these magic-sized QDs are reasonably well dispersed in the nematic host, and finally that some domains show more significant QD aggregation than others.

Acknowledgements

This work was financially supported by the Natural Science and Engineering Research Council (NSERC) of Canada, the Canada Foundation for Innovation (CFI), the Manitoba Research and Innovation Fund (MRIF), The University of Manitoba's Technology Transfer Office (NSERC/CIHR Intellectual Property Mobilization), the Deutsche Forschungsgemeinschaft (DFG, KI 411), the European Science Foundation (ESF-EUROCORES, SONS II program, LCNANOP project), and by the National Research Council (NRC) of Canada. The authors would like to thank A. Billy and Md Badruz Zaman (at the Steacie Institute for Molecular Science) for the synthesis of the quantum dots, and Dr X. Wu for the TEM analysis of **QD3**. Finally, we are grateful for the help of Dr K. McEleney (Chemistry, University of Manitoba) for XPS measurements on the quantum dots, and Dr M. S. Freund for access to the XPS instrument.

Notes and references

1 P.-G. de Gennes, *The Physics of Liquid Crystals*, 1974, Clarendon Press, Oxford.
2 J. Leys, C. Glorieux and J. Thoen, *Phys. Rev. E: Stat., Nonlinear, Soft Matter Phys.*, 2008, **77**, 061707.
3 G. Cordoyiannis, S. Kralj, G. Nounesis, Z. Kutnjak and S. Žumer, *Phys. Rev. E: Stat., Nonlinear, Soft Matter Phys.*, 2007, **75**, 021702.
4 S. A. Różański and J. Thoen, *Liq. Cryst.*, 2005, **32**, 331–340.
5 A. V. Zakharov and J. Thoen, *Eur. Phys. J. E: Soft Matter Biol. Phys.*, 2005, **17**, 447–453.
6 L. Dolgov, O. Yaroshchuk and M. Lebovka, *Mol. Cryst. Liq. Cryst.*, 2008, **496**, 212–229.
7 E. M. Jo, A. K. Srivastava, J. J. Bae, M. Kim, M.-H. Lee, H. K. Lee, S.-E. Lee, S. H. Lee and Y. H. Lee, *Mol. Cryst. Liq. Cryst.*, 2009, **498**, 74–82.
8 R. Basu and G. S. Iannacchione, *Appl. Phys. Lett.*, 2008, **93**, 183103–183105.
9 I. Dierking, K. Casson and R. Hampson, *Jpn. J. Appl. Phys.*, 2008, **47**, 6390–6393.
10 C. Huang, Y. Lin and Y. Huang, *Jpn. J. Appl. Phys.*, 2008, **47**, 6407–6409.
11 J. Y. Kim, D. K. Kim and S. H. Kim, *Eur. Polym. J.*, 2009, **45**, 316–324.
12 H. Qi and T. Hegmann, *J. Mater. Chem.*, 2006, **16**, 4197–4205.
13 F. H. Li, O. Buchnev, C. Il Cheon, A. Glushchenko, V. Reshetnyak, Y. Reznikov, T. J. Sluckin and J. L. West, *Phys. Rev. Lett.*, 2006, **97**, 147801.
14 (*a*) T. Hegmann, H. Qi and V. M. Marx, *J. Inorg. Organomet. Polym. Mater.*, 2007, **17**, 483–508; (*b*) H. Qi and T. Hegmann, *J. Mater. Chem.*, 2008, **18**, 3288–3294, and references cited in both.
15 O. Stamatoiu, J. Mirzaei, X. Feng and T. Hegmann, *Top. Curr. Chem.*, 2011, DOI: 10.1007/128_2011_233.
16 S. Kobayashi, T. Miyama, N. Nishida, Y. Sakai, H. Shiraki, Y. Shiraishi and N. Toshima, *J. Disp. Technol.*, 2006, **2**, 418.
17 (*a*) I. Dierking, G. Scalia, P. Morales and D. LeClere, *Adv. Mater.*, 2004, **16**, 865–869; (*b*) S. Schmyra, M. Kühnast, V. Lutz, S. Jagiella, U. Dettlaff-Weglikowska, S. Roth, F. Giesselmann, C. Tschierske, G. Scalia and J. Lagerwall, *Adv. Funct. Mater.*, 2010, **20**, 3350–3357; (*c*) For a review on carbon nanotube-LC dispersions, see: G. Scalia, *ChemPhysChem*, 2010, **11**, 333–340.
18 L. O. Dolgov and O. V. Yaroshchuk, *Colloid Polym. Sci.*, 2004, **282**, 1403–1408.
19 F. Haraguchi, K. I. Inoue, N. Toshima, S. Kobayashi and K. Takatoh, *Jpn. J. Appl. Phys.*, 2007, **46**, L796–L797.
20 I. C. Khoo, D. H. Werner, X. Liang, A. Diaz and B. Weiner, *Opt. Lett.*, 2006, **31**, 2592–2594.
21 O. Rivoire and J. Barre, *Phys. Rev. Lett.*, 2006, **97**, 148701.
22 Y. Shiraishi, N. Toshima, K. Maeda, H. Yoshikawa, J. Xu and S. Kobayashi, *Appl. Phys. Lett.*, 2002, **81**, 2845–2847.
23 T. Miyama, J. Thisayukta, H. Shiraki, Y. Sakai, Y. Shiraishi, N. Toshima and S. Kobayashi, *Jpn. J. Appl. Phys.*, 2004, **43**, 2580–2584.
24 N. Nishida, Y. Shiraishi, S. Kobayashi and N. Toshima, *J. Phys. Chem. C*, 2008, **112**, 20284–20290.
25 B. Kinkead and T. Hegmann, *J. Mater. Chem.*, 2010, **20**, 448–458.
26 H. Qi, B. Kinkead and T. Hegmann, *Adv. Funct. Mater.*, 2008, **18**, 212–221.
27 H. Qi and T. Hegmann, *ACS Appl. Mater. Interfaces*, 2009, **1**, 1731–1738.
28 H. Qi, B. Kinkead and T. Hegmann, *Proc. SPIE*, 2008, **6911**, 691106.
29 M. Urbanski, B. Kinkead, H. Qi, T. Hegmann and H.-S. Kitzerow, *Nanoscale*, 2010, **2**, 1118–1121.
30 J. Ouyang, M. B. Zaman, F. J. Yan, D. Johnston, G. Li, X. Wu, D. Leek, C. I. Ratcliffe, J. A. Ripmeester and K. Yu, *J. Phys. Chem. C*, 2008, **112**, 13805–13811.
31 K. Yu, Z. M. Hu, R. Wang, M. Le Piolet, M. Frotey, Md. B. Zaman, X. Wu, D. Leek, Y. Tao, D. Wilkinson and C. Li, *J. Phys. Chem. C*, 2010, **114**, 3329–3339.
32 For TEM analysis (data in Table 1), XPS, and UV-vis see ESI†, for PL spectrophotometry, see Fig. 1 and K. Yu et al., (manuscript in preparation).
33 S. T. Wu, D. Coates and E. Bartmann, *Liq. Cryst.*, 1991, **10**, 635–646.
34 Mixtures of **QD1** and **QD3** in **LC1** at 1 wt% show similar steep slope changes as pure **LC1** in transmission *vs.* applied voltage scans allowing for an easy determination of V_{th}. Mixtures at higher QD concentrations (2.5 to 5 wt%) feature a more gradual increase in the slope of intensity *vs.* applied voltage (see ESI†) and lower values for V_{th} can be derived. For QD1, however, the lowest V_{th} is observed for the 2.5 wt% mixture in **LC1**. For **QD3**, V_{th} decreases gradually with increasing QD concentration in **LC1**.
35 I. I. Smalyukh, S. V. Shiyanovskii and O. D. Lavrentovich, *Chem. Phys. Lett.*, 2001, **336**, 88–96.
36 M. Urbanski, B. Kinkead, T. Hegmann and H. S. Kitzerow, *Liq. Cryst.*, 2010, **37**, 1151–1156.
37 B. Kinkead, M. Urbanski, H. Qi, H.-S. Kitzerow and T. Hegmann, *Proc. SPIE*, 2010, **7775**, 777511.
38 M. Draper, I. M. Saez, S. J. Cowling, P. Gai, B. Heinrich, B. Donnio, D. Guillon and J. W. Goodby, *Adv. Funct. Mater.*, 2011, **21**, 1260–1278.
39 V. G. Nazarenko, R. Klouda and O. D. Lavrentovich, *Phys. Rev. E: Stat. Phys., Plasmas, Fluids, Relat. Interdiscip. Top.*, 1998, 57, R36–R38.

